

NODYCON Conference Proceedings Series

Walter Lacarbonara *Editor*

Advances in Nonlinear Dynamics, Volume II

Proceedings of the Third International
Nonlinear Dynamics Conference
(NODYCON 2023)

 Springer

NODYCON Conference Proceedings Series

Series Editor

Walter Lacarbonara, Sapienza University of Rome, Rome, Italy

The NODYCON Conference Proceedings Series presents early findings and case studies from a wide range of fundamental and applied work across the range of multidisciplinary fields that encompass Nonlinear Dynamics. Series volumes follow the principle tracks or focus topics featured in the biennial International Nonlinear Dynamics Conference. Volumes in the series feature both well-established streams of research as well as novel areas and emerging fields of investigation.


Walter Lacarbonara
Editor

Advances in Nonlinear Dynamics, Volume II

Proceedings of the Third International
Nonlinear Dynamics Conference
(NODYCON 2023)

 Springer

Editor

Walter Lacarbonara 
Department of Structural and Geotechnical
Engineering
Sapienza University of Rome
Rome, Italy

ISSN 2730-7689 ISSN 2730-7697 (electronic)
NODYCON Conference Proceedings Series
ISBN 978-3-031-50638-3 ISBN 978-3-031-50639-0 (eBook)
<https://doi.org/10.1007/978-3-031-50639-0>

© The Editor(s) (if applicable) and The Author(s), under exclusive license to Springer Nature Switzerland AG 2024

This work is subject to copyright. All rights are solely and exclusively licensed by the Publisher, whether the whole or part of the material is concerned, specifically the rights of translation, reprinting, reuse of illustrations, recitation, broadcasting, reproduction on microfilms or in any other physical way, and transmission or information storage and retrieval, electronic adaptation, computer software, or by similar or dissimilar methodology now known or hereafter developed.

The use of general descriptive names, registered names, trademarks, service marks, etc. in this publication does not imply, even in the absence of a specific statement, that such names are exempt from the relevant protective laws and regulations and therefore free for general use.

The publisher, the authors, and the editors are safe to assume that the advice and information in this book are believed to be true and accurate at the date of publication. Neither the publisher nor the authors or the editors give a warranty, expressed or implied, with respect to the material contained herein or for any errors or omissions that may have been made. The publisher remains neutral with regard to jurisdictional claims in published maps and institutional affiliations.

This Springer imprint is published by the registered company Springer Nature Switzerland AG
The registered company address is: Gewerbestrasse 11, 6330 Cham, Switzerland

Paper in this product is recyclable.

Preface

This volume is part of three volumes collecting the *Proceedings of the Third International Nonlinear Dynamics Conference (NODYCON 2023)* held in Rome from June 18 to 22, 2023. NODYCON originated in 2019 with the purpose of continuing the tradition of a conference series initiated by Prof. Ali H. Nayfeh in 1986 at Virginia Tech, known as the Nonlinear Vibrations, Stability, and Dynamics of Structures Conference. After the passing of Prof. Nayfeh in 2017, NODYCON 2019 evolved into a collective tribute to his enduring contributions. The conference received an outstanding response from the community, with 450 submissions and around 400 participants representing 68 countries.

Following the launch of NODYCON in 2019, NODYCON 2021, originally scheduled to take place in Rome on February 16–19, 2021, underwent a transformation into a virtual (online) conference in response to the widespread uncertainties arising from the global pandemic.

In June 2023, NODYCON 2023 reconvened in Rome after four years from the inaugural event, providing participants with both in-person and online presentation formats. Driven by a strong commitment to promoting personal connections and the exchange of scientific ideas together with meaningful social interactions, the conference successfully brought together a diverse community of over 600 participants. The Organizing Committee, comprised of 21 members, reviewed 577 abstracts, ultimately approving the presentation and publication of 557 one-page abstracts, accompanied by posters, into the Conference Book of Abstracts, following standard review cycles.

To structure the technical sessions, the diverse topics explored in the papers were categorized into four overarching themes:

- A – Concepts and methods in nonlinear dynamics
- B – Nonlinear dynamics of mechanical and structural systems
- C – Nonlinear dynamics and control
- D – Recent trends in nonlinear dynamics

The authors of a selection of approximately 50 papers were invited to publish in the Special Issue of *Nonlinear Dynamics* entitled “NODYCON 2023 Third

International Nonlinear Dynamics Conference”. At the same time, about 171 full papers were submitted to *Advances in Nonlinear Dynamics – Proceedings of the Third International Nonlinear Dynamics Conference (NODYCON 2023)* within the *NODYCON Conference Proceedings Series*. After a rigorous peer review process, 146 papers were accepted. These papers have been collected into three volumes, which are listed below together with a sub-topical organization.

Volume 1: Nonlinear Dynamics of Structures, Systems and Devices

- (i) Fluid-structure interactions
- (ii) Mechanical systems and structures
- (iii) Computational nonlinear dynamics
- (iv) Analytical techniques
- (v) Bifurcation and dynamic instability
- (vi) Rotating systems
- (vii) Nonsmooth systems
- (viii) Experimental dynamics

Volume 2: Nonlinear Dynamics and Control

- (i) Control of nonlinear systems
- (ii) Synchronization
- (iii) Nonlinear vibration control
- (iv) Sensors and actuators
- (v) Passive energy damping

Volume 3: New Trends in Nonlinear Dynamics

- (i) MEMS/NEMS
- (ii) Chaotic systems and uncertainty
- (iii) Energy harvesting
- (iv) Constitutive and phenomenological models
- (v) Fractional-order systems
- (vi) System identification and SHM
- (vii) Nonlinear wave propagation
- (viii) Nonlinear phenomena in bio- and eco-systems dynamics

The success of NODYCON 2023 can be attributed to the collective efforts, talent, energy, and enthusiasm of the entire community of researchers in the field of nonlinear dynamics. Their dynamic contributions were reflected in the vibrant writing, submission, and presentation of papers. Special praise is also extended to the handling editors, drawn from the Organizing, Steering, and Advisory Boards, and the hardworking reviewers. Their dedicated commitment to reading, examining, and evaluating numerous papers played a pivotal role in ensuring a high standard of quality for the conference proceedings.

Rome, Italy
December 2023

Walter Lacarbonara

Preface for Volume 2: Nonlinear Dynamics and Control

Volume 2 of the NODYCON 2023 Proceedings is composed of 25 papers, which are spread across the following groupings: (i) control of nonlinear systems (10 papers), (ii) synchronization (3 papers), (iii) nonlinear vibration control (6 papers), (iv) sensors and actuators (2 papers), (v) passive energy damping (4 papers). Due to the cross-cutting nature of the topics, the editor acknowledges that a paper placed in one grouping could have easily been placed in another grouping as well. As one reads through these 25 contributions, one will note the use of a wide range of experimental, analytical, and numerical techniques for study of nonlinear control techniques aimed at *synchronization*, vibration suppression, disturbance rejection, response optimization.

In Part I dealing with *control of nonlinear systems*, the application of super twisting sliding mode control for the synchronous reluctance motor control system is explored by J. Moon et al. Vibration control of time-varying nonlinear systems is investigated by A. Alshaya. Power consumption improvement in position and attitude control of spacecraft using electromagnetic force assist is addressed by H. Gutierrez. Nonlinear dynamic behavior and control of a third-order Duffing oscillator with external force are discussed by J. M. Balthazar et al. Motion control of a pendulum via magnetic interaction is studied by P. Atzampou et al. Image-based aerial grasping of a moving target based on model predictive control is investigated by M. Moghanipour and A. Banazadeh. The efficiency study of the non-instantaneous double support phase in HZD controlled bipedal robot is conducted by Y. Luo et al. Aeroelastic limit cycle oscillations due to a multi-element control surface with freeplay are investigated by L. D. W. Lopes et al. The complete bifurcation analysis of a buck converter under current mode control is conducted by A. Ipatovs et al. The problem of reversing along a curved path by an autonomous truck–semitrailer combination is tackled by L. Mihalyi and D. Takacs.

In Part II, the *synchronization* of fractional discrete-time complex networks with time delays via an event-triggered strategy is investigated by X. Yuan et al. The mirroring of synchronization in a multilayer configuration of Kuramoto oscillators is studied by D. Biswas and S. Gupta. Synchronization based on intermittent sampling

in PWL multiscroll systems is explored by J. L. Echeausía Monroy and J. Pena Ramirez.

Part III addresses various problems of *nonlinear vibration control*. The design method for hoist stabilization is presented by D. Reineke et al. The exact closed-form expressions for optimum inertial amplifier nonlinear friction bearing isolators are derived by S. Chowdhury et al. Control of an acoustic mode by a digitally created nonlinear electroacoustic absorber at low excitation levels is experimentally demonstrated by M. Morell et al. Preliminary numerical analysis of vibro-impact isolation systems under seismic excitations is carried out by G. Perna et al. The maneuvering of a stick in three-dimensional space using impulsive forces is explored by A. Khandelwal et al. The mitigation of vibration levels of mistuned cyclic structures by the use of contact nonlinearities is investigated by S. Quaegebeur et al.

In Part IV addressing *sensors and actuators*, the shape of a deformed PVDF wearable pressure sensor is evaluated by M. Naghdi and H. Zhang through the analysis of an acoustic traveling wave. Sound sensing with electrospun piezo materials on a 3D-printed structure is explored by G. Lanzara and K. C. Chinnam.

Passive energy damping is discussed in a series of papers in Part V. Rotor vibration mitigation is achieved by M. Selwanis et al. through the use of free balls in non-rotating tracks. The nonlinear mode approximation for vibro-impact NES is investigated by B. Youssef and R. Leine using the multiple scales method. Vibration damping in fiber-reinforced bistable composites with magnetic particles is studied by G. Lanzara et al. The interaction between magnetic fields and ferrite particles for membranes with augmented shock-absorption capability is explored by G. Lanzara et al.

We hope that readers will find valuable insights from the diverse research presented herein, focusing on the interplay between controls and nonlinear dynamics. We trust that this collection of work will not only serve as a source of knowledge but also act as a catalyst, sparking new ideas and motivating future contributions to this field.

Rome, Italy
December 2023

Walter Lacarbonara

Contents

Part I Control of Nonlinear Systems

Super-Twisting Sliding Mode Control with Accelerated Gradient Descent Method for Synchronous Reluctance Motor Control System	3
Hyunwoo Kim and Jun Moon	
Vibration Control of Time-Varying Nonlinear Systems	15
Abdullah A. Alshaya	
Power Consumption Improvement in Position and Attitude Control of Spacecraft Using Electromagnetic Force Assist	25
Hector Gutierrez, Solenne Lameaud, and Oceane Topenot	
Some Comments on Nonlinear Dynamic Behavior and Control of a 3rd-order Duffing Oscillator with External Force	37
Mauricio A. Ribeiro, Hilson H. Daum, Angelo M. Tusset, and Jose M. Balthazar	
Motion Control of a Pendulum via Magnetic Interaction	49
Panagiota Atzampou, Peter Meijers, Apostolos Tsouvalas, and Andrei Metrikine	
Image-Based Aerial Grasping of a Moving Target Using Model Predictive Control	61
M. Moghanipour and A. Banazadeh	
Efficiency Study of the Non-instantaneous Double Support Phase in HZD Controlled Bipedal Robot	73
Yinnan Luo, Ulrich J. Römer, Marten Zirkel, Lena Zentner, and Alexander Fidlin	
Aeroelastic Limit Cycle Oscillations Due to Multi-element Control Surface with Freeplay	83
Larissa D. Wayhs-Lopes, Douglas D. Bueno, and Carlos E. S. Cesnik	

The Complete Bifurcation Analysis of Buck Converter Under Current Mode Control	95
Iheanacho Chukwuma Victor, Sergejs Tjukovs, Aleksandrs Ipatovs, Daniils Surmacs, and Dmitrijs Pikulins	
Reversing Along a Curved Path by an Autonomous Truck–Semitrailer Combination	105
Levente Mihályi and Dénes Takács	
Part II Synchronization	
Synchronization of Fractional Discrete-Time Complex Networks with Time Delays via Event-Triggered Strategy	119
Xiaolin Yuan, Guojian Ren, Yongguang Yu, and Wei Chen	
Mirroring of Synchronization in Multilayer Configuration of Kuramoto Oscillators	131
Dhrubajyoti Biswas and Sayan Gupta	
Synchronization Based on Intermittent Sampling: PWL Multiscroll System	143
José Luis Echenausía-Monroy and Jonatan Pena-Ramirez	
Part III Nonlinear Vibration Control	
Hoist Stabilization Design Method	155
David Reineke, Duy (Kyle) Nguyen, Luyi Tang, M. Lanzerotti, and W. Lacarbonara	
The Exact Closed-Form Expressions for Optimum Inertial Amplifier Coupled Nonlinear Friction Bearing Isolators	165
Sudip Chowdhury, Arnab Banerjee, and Sondipon Adhikari	
Control of an Acoustic Mode by a Digitally Created Nonlinear Electroacoustic Absorber at Low Excitation Levels: Experimental Results	177
Maxime Morell, Manuel Collet, Emmanuel Gourdon, Alireza Ture Savadkoohi, and Emanuele De Bono	
Preliminary Numerical Analysis of the Vibro-Impact Isolation Systems Under Seismic Excitations	189
Giuseppe Perna, Maurizio De Angelis, and Ugo Andreas	
Maneuvering a Stick in Three-Dimensional Space Using Impulsive Forces	199
Aakash Khandelwal, Nilay Kant, and Ranjan Mukherjee	
Mitigating Vibration Levels of Mistuned Cyclic Structures by Use of Contact Nonlinearities	211
Samuel Quaegebeur, Benjamin Chouvion, and Fabrice Thouverez	

Part IV Sensors and Actuators

Evaluating the Shape of a Deformed PVDF Wearable Pressure Sensors by Analyzing an Acoustic Traveling Wave..... 223

Masoud Naghdi and Haifeng Zhang

Sensing Sound with Electrospun Piezo Materials on a 3D-Printed Structure 233

Krishna Chytanya Chinnam and Giulia Lanzara

Part V Passive Energy Damping

Free Balls in a Non-rotating Track Can Mitigate Rotor Vibration 245

Michael M. Selwanis, Mohammed M. Ibrahim, Mohamed S. Khadr, and Ahmed F. Nemnem

Vibro-Impact NES: Nonlinear Mode Approximation Using the Multiple Scales Method..... 255

Balkis Youssef and Remco I. Leine

Vibration Damping in Fiber-Reinforced Bistable Composites with Magnetic Particles..... 267

Alessandro Porrari and Giulia Lanzara

Magnetic Field and Ferrite Particles Interaction for Membranes with Augmented Shock-Absorption Capability 279

Stefania Fontanella, Ginevra Hausherr, Shiela Meryl Cumayas Cabral, Antonio Loisi, and Giulia Lanzara

Index 291

Part I
Control of Nonlinear Systems

Super-Twisting Sliding Mode Control with Accelerated Gradient Descent Method for Synchronous Reluctance Motor Control System



Hyunwoo Kim and Jun Moon

1 Introduction

Synchronous reluctance motors (SynRMs) have received considerable attention in various applications due to its high efficiency and low cost, compared to other types of motors such as induction motors (IMs) and permanent magnet synchronous motors (PMSMs) [1]. However, IMs cannot guarantee the high efficiency due to additional secondary copper loss. Although PMSMs show the remarkable performance such as the torque density and efficiency, they are less cost competitive than SynRMs due to the presence of the rare-earth PM in the former. There are several attempts to replace IMs and PMSMs with SynRMs [2].

The general SynRM control system consists of the speed and current controller and current vector algorithm. Proportional-integral (PI) controller is widely used in the speed and current controllers of conventional SynRM control systems (see Fig. 1). However, a satisfactory control performance may not be guaranteed due to the presence of nonlinearities, uncertainties, and disturbances in the system [3]. To resolve these issues, speed and current controllers were designed using the sliding mode control (SMC) approach [4–9]. However, [4–6] used the first-order SMC method; hence, their motor control systems suffer from the high chattering phenomenon. In [7], the adaptive terminal sliding mode reaching law is used to improve the reaching time and reduce the chattering effect. In addition, [8] used the super-twisting SMC (STSMC) approach to reduce the chattering effect of the first-order SMC in [4, 5]. In [9], a robust stator current controller in induction motor

H. Kim (✉)

Research Institute of Industrial Science, Hanyang University, Seoul, South Korea
e-mail: khw7481@hanyang.ac.kr

J. Moon

Department of Electrical Engineering, Hanyang University, Seoul, South Korea
e-mail: junmoon@hanyang.ac.kr

is proposed using the discrete-time super-twisting current control for reducing the chattering and the control effect. However, the controllers in [8, 9] are discontinuous due to the presence of the sign function. We also note that [4–9] did not consider the SynRM control system. In the current vector control algorithm, the current phase angle is determined by the particular control objective. There are various current vector control algorithms such as the maximum torque per ampere (MTPA) control, flux weakening (FW) control, the maximum torque per voltage (MTPV) control, the maximum power factor control (MPFC), and the maximum efficiency control (MEC) [10–12]. This class of algorithms is heavily dependent on the motor parameters (see Table 1). However, the motor parameters generally have nonlinear characteristics due to the magnetic saturation [13, 14]. Lookup tables (LUTs) based on finite element analysis (FEA) have been used to cope with nonlinearities in motor parameters. Using LUTs, the optimal current vector can be determined through various methods such as the signal injection method [15, 16], neural network method [12], and gradient descent method [17].

The main contributions of the study are as follows:

- (a) In the speed controller, since our STSMC is a continuous, the SynRM control system achieves the fast dynamic response under disturbance. Moreover, we provide a detailed analysis of the finite-time reachability of the proposed STSMC. The proposed STSMC guarantees asymptotic stability during the sliding phase. Through experimental testing, we demonstrated that the proposed SynRM control system achieves the fast dynamic response.
- (b) In current vector control, AGDM is proposed to achieve high-efficiency operation under the nonlinear characteristics of SynRM. Specifically, MTPA was applied to obtain a fast dynamic response in the transient state, and MEC is used for high-efficiency operation in the steady state. LUTs based on FEA are adopted due to the nonlinear characteristics by the magnetic saturation. We propose AGDM based on LUT to quickly search for the optimal current vector subject to the limited computation time of DSP.
- (c) The proposed STSMC-AGDM was implemented in a 500W SynRM control system. Specifically, in Sect. 4, the proposed control scheme shows the better speed control performance and motor efficiency, compared with the conventional PI control with/without AGDM and STSMC without AGDM.

2 Conventional Control System of SynRM

2.1 Mathematical SynRM Model

In the synchronous frame, the voltage equation of SynRM with the iron loss is given by $v_d = R_s i_d - \omega_e L_q (1 + R_s/R_c) i_q$ and $v_q = R_s i_q + \omega_e L_d (1 + R_s/R_c) i_d$, where v_d and v_q are the dq -axis voltage, i_d and i_q are the dq -axis current, R_s

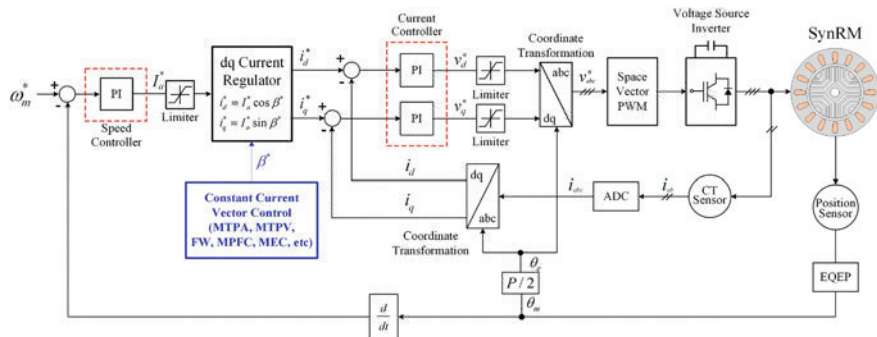


Fig. 1 Block diagram of the conventional control system

is the armature resistance, R_c is the iron loss resistance, L_d and L_q are the dq -axis inductance, respectively, and ω_e is the synchronous speed. The torque and mechanical equations of SynRM are expressed as follows:

$$T_e = (3P/4)(L_d - L_q)i_d i_q = J_m (d\omega_m/dt) + B_m \omega_m + T_L, \quad (1)$$

where T_e is the reluctance torque of SynRM, P is the number of poles, J_m is the system inertia, ω_m is the mechanical speed, B_m is the friction coefficient, and T_L is the load torque. The efficiency (η) of SynRM is determined as follows:

$$\eta = \frac{T_e \omega_m}{T_e \omega_m + W_c + W_i}, \quad W_c = \frac{3}{2} R_s (i_d^2 + i_q^2), \quad W_i = \frac{3}{2} \omega_e^2 \frac{(L_d i_d)^2 + (L_q i_q)^2}{R_c}, \quad (2)$$

where W_c is the copper loss and W_i is the iron loss.

2.2 Conventional SynRM Control System

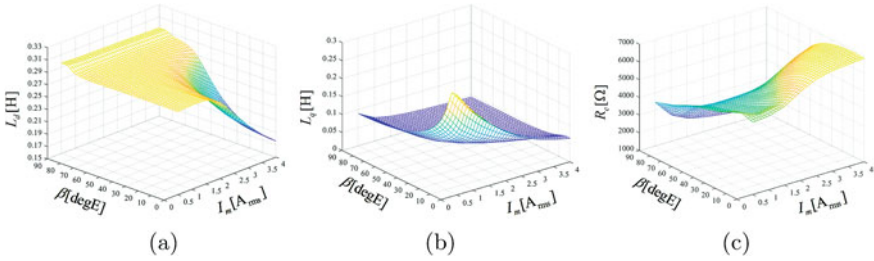
Figure 1 shows the conventional SynRM control system. Here, PI controller is used to control both speed and current. The output of speed control is the magnitude of current, and the current phase angle is determined by the current vector algorithm. Table 1 shows the current phase angle according to the control objective. Based on the magnitude and phase angle of current, the command of dq -axis current was computed as $i_d^* = I_m \cos \beta$ and $i_q^* = I_m \sin \beta$. Thereafter, the dq -axis voltage command was computed using the current controller. The three-phase voltage was applied to SynRM (or PMSM, IM) using the voltage source inverter (VSI) by space vector pulse width modulation (SVPWM).

Table 1 Current phase angle according to control methods

Control method	Description	$\tan \beta$
MTPA	Maximum torque per ampere	1
MTPV	Maximum torque per voltage	L_d/L_q
MPFC	Maximum power factor control	$\sqrt{L_d/L_q}$
MEC	Maximum efficiency control	$\sqrt{\frac{R_s R_c^2 + \omega_e^2 L_q^2 (R_s + R_c)}{R_s R_c^2 + \omega_e^2 L_d^2 (R_s + R_c)}}$

Table 2 Specification of SynRM

Parameters	Quantities
Number of poles/slots	4/36
Rated power/speed	500[W]/1500[r/min]
Rated voltage/current	380[V]/3.5[A]
d -axis/ q -axis inductance (at rated current)	272.2[mH]/48.05[mH]
Stator/iron loss resistance	5.05[Ω]/1500[Ω]
Switching frequency	10[kHz]

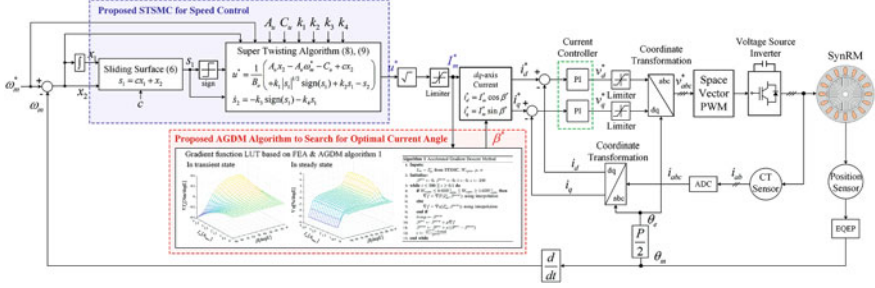
**Fig. 2** Nonlinear characteristics of SynRM according to the current vector. (a) d -axis inductance. (b) q -axis inductance. (c) Iron loss resistance

2.3 Nonlinear Characteristics of SynRM

The characteristics of SynRM are determined by the dq -axis inductances denoted by L_d and L_q as shown in (1) and (2). The dq -axis inductances L_d and L_q are functions of the relative permeability. Since the relative permeability in the electrical steel has a nonlinear characteristic, the dq -axis inductances of SynRM have the nonlinear characteristics according to the current vector. For the analysis of the nonlinear characteristics, ANSYS Maxwell 2021R1 was used as FEA program. Table 2 shows the specifications of SynRM. Figure 2a,b,c shows the parameters of SynRM for the current vector. The motor parameters of SynRM have the nonlinear characteristics (Table 3).

Table 3 Parameters of the controllers

Controller	Parameters
PISC	$K_{ps} = 0.006, K_{is} = 10^{-5}$
PI current controller	$K_{pc} = 58, K_{ic} = 0.0008$
STSMC	$k_1 = 0.001, k_2 = 0.04, k_3 = 0.008, k_4 = 10^{-7}$
AGDM	$\mu = 50, \kappa = 0.25$

**Fig. 3** Block diagram of the proposed SynRM control system

3 Proposed Speed and Current Vector Control

Figure 3 shows the proposed STSMC-AGDM-based control system. Unlike the conventional control system shown in Fig. 1, we design STSMC as the speed controller and applies AGDM to search for the optimal current vector. Specifically, in Fig. 3, the proposed STSMC is used for speed control, whereas the proposed AGDM is applied to optimal current vector control. The other blocks in Fig. 3, including the dq -axis current, proportional-integrator (PI) current controller, limiters, coordinate transformation, ADCs, voltage source inverter, and sensors, are standard implementation used in various motor control systems.

3.1 STSMC for Speed Control

We propose STSMC for speed control to achieve a fast dynamic response (see Fig. 3). The dynamic equation of the SynRM control system is

$$\dot{\omega}_m = A_u \omega_m + B_u u^* + C_u, \quad (3)$$

where $A_u = -B_m/J_m$, $B_u = \frac{3P}{8J_m} (L_d - L_q) \sin 2\beta$, $C_u = -T_L/J_m$, and $u = I_a^{*2}$. From (3), the speed error and its derivative are $x_1 = e_\theta = \theta_m^* - \theta_m$ and $x_2 = \dot{x}_1 = \omega_m^* - \omega_m$. We propose a sliding surface defined by $s_1 = cx_1 + x_2$ where $c > 0$. The derivative of the sliding surface is given as follows:

$$\dot{s}_1 = c\dot{x}_1 + \dot{x}_2 = cx_2 + (A_u x_2 - A_u \omega_m^* - B_u u^* - C_u). \quad (4)$$

The control input of the proposed STSMC is designed as follows:

$$\begin{aligned} u^* &= \frac{1}{B_u} (A_u x_2 - A_u \omega_m^* - C_u + c\dot{x}_1 + k_1 |s_1|^{1/2} \text{sign}(s_1) + k_2 s_1 - s_2) \\ \dot{s}_2 &= -k_3 \text{sign}(s_1) - k_4 s_1, \end{aligned} \quad (5)$$

where k_1, k_2, k_3 , and k_4 are positive design constants and $c > 0$. By substituting (5) into (4), the derivative of the sliding surface can be expressed as follows:

$$\dot{s}_1 = -k_1 |s_1|^{1/2} \text{sign}(s_1) - k_2 s_1 + s_2, \quad \dot{s}_2 = -k_3 \text{sign}(s_1) - k_4 s_1.$$

Theorem 1 Consider the SynRM control system in (3) with the proposed STSMC in (5). The following properties hold:

- (1) The finite-time reachability is achieved if the following conditions are satisfied: $k_i > 0, i = 1, \dots, 4$ and $4k_3 k_4 < (8k_3 + 9k_1^2)k_2^2$, where the explicit finite time is given by $T = \frac{2}{\gamma_2} \ln(1 + \frac{\gamma_2}{\gamma_1} v^{1/2}(0))$.
- (2) Furthermore, after the finite-time reachability given in part (1), the asymptotic stability is achieved.

Proof We only prove the finite-time reachability in part (1). We consider the following Lyapunov function: $V = 2k_3 |s_1| + k_4 s_1^2 + \frac{1}{2} s_2^2 + \frac{1}{2} (k_1 |s_1|^{1/2} \text{sign}(s_1) + k_2 s_1 - s_2)^2$. Define $\zeta = [|s_1|^{1/2} \text{sign}(s_1) \quad s_1 \quad s_2]^T$. Then the derivative of Lyapunov function can be expressed as $\dot{V} = -\frac{1}{|s_1|^{1/2}} \zeta^T K_1 \zeta - \zeta^T K_2 \zeta$, where

$$\begin{aligned} K_1 &= \begin{bmatrix} \frac{1}{2} k_1^3 + k_1 k_3 & 0 & -\frac{1}{2} k_1^2 \\ 0 & k_4 k_1 + \frac{5}{2} k_2^2 k_1 & -\frac{3}{2} k_1 k_2 \\ -\frac{1}{2} k_1^2 & -\frac{3}{2} k_1 k_2 & \frac{1}{2} k_1 \end{bmatrix}, \\ K_2 &= \begin{bmatrix} k_2 k_3 + 2k_1^2 k_2 & 0 & 0 \\ 0 & k_4 k_2 + k_2^3 - k_2^2 \\ 0 & -k_2^2 & k_2 \end{bmatrix}. \end{aligned}$$

We can easily see that $\dot{V} < 0$ if K_1 and K_2 are positive definite. These conditions are satisfied by Theorem 1-(1). Then when $\dot{V} < 0$ holds, we can show that $\dot{V} \leq -\gamma_1 V^{1/2} - \gamma_2 V$, where γ_1 and γ_2 are positive constants. Note that the solution of $\dot{v} = -\gamma_1 v^{1/2} - \gamma_2 v$ with $v(0) > 0$ is given by $v(t) = e^{-\gamma_2 t} [v^{1/2}(0) + \frac{\gamma_1}{\gamma_2} (1 - e^{\frac{\gamma_2}{2} t})]^2$. Then by the comparison principle, the sliding variable converges to zero in finite time, where the corresponding finite time can be obtained as $T = \frac{2}{\gamma_2} \ln(1 + \frac{\gamma_2}{\gamma_1} v^{1/2}(0))$. This shows the finite-time convergence in part (1). \square

Algorithm 1 Accelerated Gradient Descent Method (AGDM)

```

1: Inputs:
    $I_m \leftarrow I_m^*$  from STSMC,  $\omega_m$ ,  $\omega_m^*$ ,  $\mu$ ,  $\kappa$ , and LUT as shown in Fig. 4
2: Initialize:
    $\beta^{pre} \leftarrow 0$ ,  $\beta^{new} \leftarrow 0$ ,  $i \leftarrow 0$ ,  $\epsilon \leftarrow 100$ ,  $\tau \leftarrow 0$ 
3: while  $i \leq 500 \parallel \epsilon \geq 0.1$  do
4:   if  $\omega_m \leq 0.95\omega_m^* \parallel \omega_m \geq 1.05\omega_m^*$  then
5:      $\nabla f = \nabla T_e(I_m^*, \beta^{new})$ ; based on LUT
6:   else
7:      $\nabla f = \nabla \eta(I_m^*, \beta^{new})$ ; based on LUT
8:   end if
9:    $\tau \leftarrow \beta^{new}$ 
10:   $\beta^{pre} \leftarrow \beta^{new} + \mu \nabla f$ 
11:   $\beta^{new} \leftarrow \beta^{pre} + \kappa (\beta^{pre} - \beta^{new})$ 
12:   $\epsilon \leftarrow \frac{|\beta^{new} - \tau|}{\beta^{new}}$ 
13:   $i \leftarrow i + 1$ 
14: end while

```

3.2 Searching Optimal Current Angle Using AGDM

For a fast dynamic response and high efficiency, an optimal current angle controller is proposed using the accelerated gradient descent method (AGDM) based on LUT obtained from FEA (see Fig. 3). A detailed analysis of AGDM can be found in [18] and the references therein. MTPA and MEC points are analyzed using FEA, and the gradient functions are computed to search for the optimal current angle to achieve the fast dynamic response and the high efficiency. The computation algorithm of the optimal current phase angle is as follows:

$$\beta_{k+1}^{pre} = \beta_k^{new} + \mu \nabla f m, \quad \beta_{k+1}^{new} = \beta_{k+1}^{pre} + \kappa (\beta_{k+1}^{pre} - \beta_k^{pre}), \quad (6)$$

where μ is the learning rate and κ is momentum of AGDM [18]. Here, β_k^{new} is the new current phase angle at the discrete time instant k implemented in DSP (see β^{new} in Algorithm 1). In (6), f can be either T_e or η , where T is torque (see (1)) and η is motor efficiency (see (2)). Then the gradient function ∇f can be either ∇T or $\nabla \eta$ (see Algorithm 1), which is computed using FEA with Fig. 4.

Algorithm 1 describes the searching algorithm of optimal current vector based on AGDM, where we modify the standard AGDM in [18] for the SynRM control system. The gradient function is selected for the feedback speed to improve the dynamic response and efficiency. In the transient state, which is defined as outside $\pm 5\%$ of speed command, the gradient function is selected as the torque gradient for control of the maximum torque to improve the dynamic response. Furthermore, in steady state, which is defined as within $\pm 5\%$ of speed command, the gradient function is selected as the efficiency gradient to improve the motor efficiency. Based on the gradient function, the magnitude of current from the proposed STSMC, and (6), the optimal current phase angle is computed for the current command

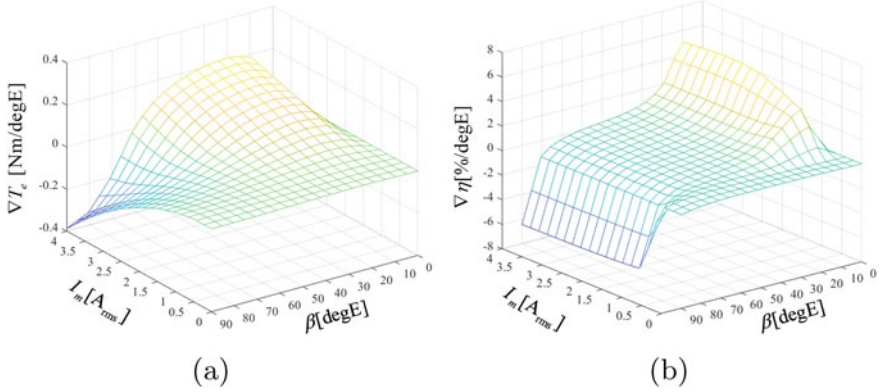


Fig. 4 Gradient function LUT based on FEA. (a) Torque. (b) Efficiency

from STSMC when the stop criterion is satisfied. The new current phase angle is computed using the gradient function and learning rate (μ). Furthermore, the momentum (κ) is used to search for the optimal current phase angle faster than the conventional gradient descent method. If the load torque is changed, the current command is changed. Subsequently, the new current angle is found via the proposed AGDM. A detailed structure of the proposed AGDM is given in Algorithm 1.

4 Experimental Results

To verify the proposed STSMC-AGDM in Sect. 3, an experiment is performed on various cases. We implement the SynRM control system structure in Fig. 3. Figure 5 shows the experimental setup, which includes a TMS320F28335 DSP board, VSI, DC power supply, PMSM load, torque sensor, 500W SynRM, control desk, oscilloscope, and power analyzer. We consider four different control schemes: (1) PI speed control with traditional MTPA [12] (PISC-TMTPA), (2) STSMC with the traditional MTPA [12] (STSMC-TMTPA), (3) PI speed control with AGDM (PISC-AGDM), and (4) the proposed STSMC-AGDM control scheme. In the experiment, the four different cases are considered:

- Case 1-1: With 1000[r/min], the load torque change from 1[Nm] to 3[Nm]
- Case 1-2: With 1200[r/min], the load torque change from 1[Nm] to 3[Nm]
- Case 2-1: With 1000[r/min], the load torque change from 3[Nm] to 1[Nm]
- Case 2-2: With 1200[r/min], the load torque change from 3[Nm] to 1[Nm]

Table 4 shows the performance comparisons of the four control schemes. The efficiency of motor is measured using the power analyzer in YOKOGAWA as shown

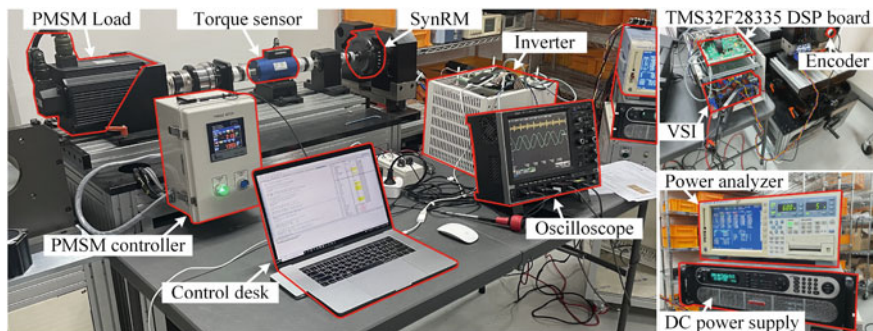


Fig. 5 Experimental setup

Table 4 Performance comparison of four control schemes

Content	PISC-TMTPA	STSMC-TMTPA	PISC-AGDM	Proposed STSMC-AGDM
Response time of Cases 1-1 and 2-1	2.6 [sec]	0.84 [sec]	2.56 [sec]	0.8 [sec]
Response time of Cases 1-2 and 2-2	2.66 [sec]	0.88 [sec]	2.32 [sec]	0.8 [sec]
Efficiency @ 1[Nm], 1000 [r/min]	78.97 [%]	78.97 [%]	79.3 [%]	79.27 [%]
Efficiency @ 3[Nm], 1000 [r/min]	81.29 [%]	81.29 [%]	81.52 [%]	81.54 [%]
Efficiency @ 1[Nm], 1200 [r/min]	80.21 [%]	80.22 [%]	80.56 [%]	80.57 [%]
Efficiency @ 3[Nm], 1200 [r/min]	82.24 [%]	82.24 [%]	82.38 [%]	82.39 [%]

in Fig. 5. The sensors for voltage, current, torque, and speed connect the power analyzer. In power analyzer, the input and out are computed using measured voltage, current, torque, and speed. Furthermore, the efficiency on the motor is computed as the ratio of the input and output. The proposed STSMC-AGDM scheme shows the fastest dynamic response for all cases (Cases 1-1, 1-2, 2-1, and 2-2). Moreover, for all cases, the efficiency of the proposed STSMC-AGDM scheme is superior to those of the other control schemes. Hence, with the proposed STSMC-AGDM scheme, the SynRM control system can achieve the fast dynamic response and the high motor efficiency. The detailed performance comparisons are provided in Table 4.

5 Conclusions

In this paper, the STSMC-AGDM-based SynRM control system has been proposed to achieve the fast dynamic response and high efficiency. While the fast dynamic response is obtained by STSMC, the high efficiency is achieved by applying AGDM to LUT to search for the optimal current vector. Based on the various experimental results, we have demonstrated the effectiveness of the proposed STSMC-AGDM scheme by comparing it with the results of other conventional methods. One possible future work is to consider neural network framework of the current vector control using LUT.

Acknowledgments This work was supported by the Technology Innovation Program (20018112) funded by the Ministry of Trade, Industry and Energy (MOTIE, Korea), by the National Research Foundation of Korea (NRF) grant funded by the Ministry of Science and ICT, South Korea (NRF-2021R1A2C2094350), and by Institute of Information & Communications Technology Planning and Evaluation (IITP) grant funded by the Korea government (MSIT) (No.2020-0-01373).

References

1. Stipetic, S., Zarko, D., Cavar, N.: Adjustment of rated current and power factor in a synchronous reluctance motor optimally designed for maximum saliency ratio. *IEEE Trans. Ind. Appl.* **56**(3), 2481–2490 (2020)
2. Moghaddam, R.R., Magnussen, F., Sadarangani, C.: Theoretical and experimental reevaluation of synchronous reluctance machine. *IEEE Trans. Ind. Electron.* **57**(1), 6–13 (2010)
3. El-Sousy, F.F.M.: Adaptive dynamic sliding-mode control system using recurrent RBFN for high-performance induction motor servo drive. *IEEE Trans. Ind. Informat.* **9**(4), 1922–1936 (2013)
4. Lin, F.J., Chang, C.K., Huang, P.K.: FPGA-based adaptive backstepping sliding-mode control for linear induction motor drive. *IEEE Trans. Power Electron.* **22**(4), 1222–1231 (2007)
5. Yeam, T.I., Lee, D.C.: Design of sliding-mode speed controller with active damping control for single-inverter dual-PMSM drive systems. *IEEE Trans. Power Electron.* **36**(5), 5794–5801 (2021)
6. Chen, Y. Zhu, P., Zhang P., Li, M., Wan, Z., Zhang, W.: Hybrid sliding-mode position-tracking control for servo system with external disturbance. *IEEE J. Emerg. Sel. Top. Power Electr.* **9**(5), 5478–5488 (2021)
7. Junejo, A.K., Xu, W., Mu, C., Ismail, M.M., Liu, Y.: Adaptive speed control of PMSM drive system based a new sliding-mode reaching law. *IEEE Trans. Power Electron.* **35**(11), 12110–12121 (2020)
8. Domínguez, J.R.: Discrete-time modeling and control of induction motors by means of variational integrators and sliding modes—part II: control design. *IEEE Trans. Ind. Electron.* **62**(10), 6183–6193 (2015)
9. Kali, Y., Ayala, M., Rodas, J., Saad, M., Doval-Gandoy, J., Gregor, R., Benjelloun, K.: Time delay estimation based discrete-time super-twisting current control for a six-phase induction motor. *IEEE Trans. Power Electron.* **35**(11), 12570–12580 (2020)
10. Betz, R., Lagerquist, R., Jovanovic, M., Miller, T., Middleton, R.: Control of synchronous reluctance machines. *IEEE Trans. Ind. Appl.* **29**(6), 1110–1122 (1993)

11. Ni, R., Xu, D., Wang, G., Ding, L., Zhang, G., Qu, L.: Maximum efficiency per ampere control of permanent-magnet synchronous machines. *IEEE Trans. Ind. Electron.* **62**(4), 2135–2143 (2015)
12. Lin, F.J., Huang, M.S., Chen, S.G., Hsu, C.W.: Intelligent maximum torque per ampere tracking control of synchronous reluctance motor using recurrent Legendre fuzzy neural network. *IEEE Trans. Power Electron.* **34**(12), 12080–12094 (2019)
13. Mademlis, C.: Compensation of magnetic saturation in maximum torque to current vector controlled synchronous reluctance motor drives. *IEEE Trans. Energy Convers.* **18**(3), 379–385 (2003)
14. Scalcon, F.P., Osorio, C.R.D., Koch, G.G., Gabbi, T.S., Vieira, R.P., Grundling, H.A., Oliveira, R.C.L.F., Montagner, V.F.: Robust control of synchronous reluctance motors by means of linear matrix inequalities. *IEEE Trans. Energy Convers.* **36**(2), 779–788 (2021)
15. Sun, T., Wang, J., Chen, X.: Maximum Torque Per Ampere (MTPA) control for interior permanent magnet synchronous machine drives based on virtual signal injection. *IEEE Trans. Power Electron.* **30**(9), 5036–5045 (2015)
16. Kim, S., Yoon, Y.D., Sul, S.K., Ide, K.: Maximum Torque per Ampere (MTPA) control of an IPM machine based on signal injection considering inductance saturation, *IEEE Trans. Power Electron.* **28**(1), 488–497 (2013)
17. Balamurali, A., Feng, G., Lai, C., Tjong, J., Kar, N.C.: Maximum efficiency control of PMSM drives considering system losses using gradient descent algorithm based on DC power measurement. *IEEE Trans. Energy Convers.* **33**(4), 2240–2249 (2018)
18. Nesterov, Y.: *Lectures on Convex Optimization*, 2nd edn. Springer Optimization and Its Application. **137**, (2018)

Vibration Control of Time-Varying Nonlinear Systems



Abdullah A. Alshaya

1 Introduction

The application of a control input into a time-varying nonlinear system, e.g., flexible link manipulators [1, 2], crane operation with hoisting/lowering maneuver [3–5], or pouring and filling operation [6, 7], results in unwanted transient and residual vibrations. The complexity of the dynamical model for such system and the difficulty in characterizing the system model and its parameters complicate the controlling procedure in designing the required system input. The open-loop control, especially the command shaping approach, is commonly used for vibration control with precise and accurate positioning, fast and safe operation, and without the need of installing actuators and sensors or changing the physical structure of the system [6–8].

The principle of the command shaping control is to design a special input that commands the mechanical system without inducing vibration at the end of command duration. The designing process can be based on either optimal control approach or convolving a reference input with a train of specially generated input shapers [9, 10]. The input shaping approach was applied to several vibratory systems [11] and can be applied to single and multi-degree-of-freedom systems [12]. The most drawbacks of the input shaping techniques are the dependency of the rise time of the generated impulses on the system parameters, the generated jerks in their profiles, and the sensitivity of the vibration reduction with presence of uncertainties in the system parameters. The generated profiles from the input shapers can be smoothed by convolving a smooth reference command instead of trapezoidal profile [13, 14]. Furthermore, convolving large set of input shapers designed by imposing

A. A. Alshaya (✉)

Mechanical Engineering Department, College of Engineering and Petroleum, Kuwait University, Safat, Kuwait

e-mail: abdullah.alshaya@ku.edu.kw

additional constraints enhances the insensitivity range of the generated command [15]. Even though the robust input shaper was used to control a time-varying system, the induced residual vibration was not completely suppressed [4, 16]. Therefore, to accommodate the changes in the system parameters during motion, an adaptive input shaping with time-varying changes as well as combining input shaper with frequency modulation was introduced to cancel the induced vibration from a time-variant system [17, 18].

The optimal control approach has the freedom of selecting a maneuver time that compensates between the total move time and the required vibration reduction in the transient stage. The general idea of the optimal control approach is to introduce a general system input command that is designed to satisfy some known input and system constraints. For instance, the general profile can be a sequence of multiple steps [19–21] or a continuous profile such as waveform [22] or polynomial [23]. The objective here is to extend the command shaping approach to control a time-varying nonlinear system while accommodating the changes in the system parameters during the maneuver.

2 Dynamics of Time-Varying Nonlinear System

A system with N particles defined in the space by the Cartesian coordinates x_k ($k = 1, 2, \dots, 3N$) with respect to an inertial frame is considered. Suppose that the configuration of the system is completely described by n generalized coordinates $\mathbf{q} = \{q_1 \ q_2 \ \dots \ q_n\}^T \in \mathbb{R}^{n \times 1}$ such that $x_k = x_k(\mathbf{q}, t)$. The equation of motion for the i th particle is given as [24]

$$\begin{aligned} \sum_{j=1}^n m_{ij} \ddot{q}_j + \frac{1}{2} \sum_{j=1}^n \sum_{k=1}^n \left(\frac{\partial m_{ij}}{\partial q_k} + \frac{\partial m_{ik}}{\partial q_j} - \frac{\partial m_{jk}}{\partial q_i} \right) \dot{q}_j \dot{q}_k \\ + \sum_{j=1}^n \left(\frac{\partial m_{ij}}{\partial t} + \frac{\partial a_i}{\partial q_j} - \frac{\partial a_j}{\partial q_i} \right) + \frac{\partial a_i}{\partial t} - \frac{\partial T_0}{\partial q_i} + \frac{\partial V}{\partial q_i} = Q_n \quad (1) \end{aligned}$$

$(i = 1, 2, \dots, n)$

where

$$m_{ij} = m_{ji} = \sum_{k=1}^{3N} m_k \frac{\partial x_k}{\partial q_i} \frac{\partial x_k}{\partial q_j}, \quad a_i = \sum_{k=1}^{3N} m_k \frac{\partial x_k}{\partial q_i} \frac{\partial x_k}{\partial t}, \quad T_0 = \frac{1}{2} \sum_{k=1}^{3N} m_k \left(\frac{\partial x_k}{\partial t} \right)^2$$

$V = V(\mathbf{q}, t)$ is the potential function, Q_n is the generalized force, $m_1 = m_2 = m_3$ is the mass of the first particle, (x_1, x_2, x_3) is the position of the first particle, $m_4 = m_5 = m_6$ is the mass of the second particle, (x_4, x_5, x_6) is the position of the

second particle, and so on. If the generalized constraints are time-independent, i.e., $\partial x_k / \partial t = 0$, Eq. (1) can be simplified and written in a matrix form as [6, 7]

$$\mathbf{M}(\mathbf{q}, \mathbf{P})\ddot{\mathbf{q}} + \mathbf{C}(\mathbf{q}, \dot{\mathbf{q}}, \mathbf{P})\dot{\mathbf{q}} + \mathbf{F}(\mathbf{q}, \mathbf{P})\dot{\mathbf{q}} + \mathbf{G}(\mathbf{q}, \mathbf{P}) = \mathbf{Q} \quad (2)$$

where $\mathbf{M} \in \mathbb{R}^{n \times n}$ is the inertia matrix, $\mathbf{C} \in \mathbb{R}^{n \times n}$ is the Coriolis matrix, $\mathbf{F} \in \mathbb{R}^{n \times n}$ is the consequence of the symmetry of the inertia matrix, $\mathbf{G} \in \mathbb{R}^{n \times 1}$ is the gravitational vector, $\mathbf{P} \in \mathbb{R}^{n \times 1}$ is the vector of the constant and/or time-varying parameters, and $\mathbf{Q} \in \mathbb{R}^{n \times 1}$ is the vector of the generalized forces Q_n . It is worth mentioning that the inertia matrix \mathbf{M} is symmetric positive definite matrix and the matrix $\dot{\mathbf{M}} - 2\mathbf{C} - \mathbf{F}$ is skew matrix.

2.1 Quasi-static Analysis

Assuming small oscillations where the nonlinear equations of motion, Eq. (2), can be assumed to behave linearly, and considering a short time interval $t_{k-1} \leq t \leq t_k$ where the instantaneous matrices in Eq. (2) can be assumed to be constant, Eq. (2) can be written in the time interval $t_{k-1} \leq t \leq t_k$ as

$$\mathbf{M}(\bar{t})\ddot{\mathbf{q}}_k + [\mathbf{C}(\bar{t}) + \mathbf{F}(\bar{t})]\dot{\mathbf{q}}_k + \mathbf{K}(\bar{t})\mathbf{q}_k = \mathbf{Q}(t), \quad \text{for } t_{k-1} \leq t \leq t_k \quad (3)$$

where $\mathbf{K} \in \mathbb{R}^{n \times n}$ is the stiffness matrix and \bar{t} is the average time in the time interval $t \in [t_{k-1}, t_k]$ where the matrices \mathbf{M} , \mathbf{C} , \mathbf{F} , and \mathbf{K} are evaluated. Rewriting Eq. (3) in a state-space form,

$$\frac{d}{dt} \begin{Bmatrix} \mathbf{q}_k(t) \\ \dot{\mathbf{q}}_k(t) \end{Bmatrix} = \begin{bmatrix} \mathbf{0} & \mathbf{I} \\ -\mathbf{M}^{-1}\mathbf{K} & -\mathbf{M}^{-1}[\mathbf{C} + \mathbf{F}] \end{bmatrix} \begin{Bmatrix} \mathbf{q}_k(t) \\ \dot{\mathbf{q}}_k(t) \end{Bmatrix} + \begin{Bmatrix} \mathbf{0} \\ \mathbf{M}^{-1}\mathbf{Q}(t) \end{Bmatrix} \quad (4)$$

or simply as

$$\dot{\mathbf{y}}_k(t) = \mathbf{A}(\bar{t})\mathbf{y}_k(t) + \mathbf{B}(t) \quad (5)$$

where $\mathbf{0}$ and \mathbf{I} are the null and identity matrices, respectively, and \mathbf{y}_k and \mathbf{A} are the state vector and matrices, respectively. The general solution of Eq. (4) or (5) in the time interval $t_{k-1} \leq t \leq t_k$ with a given set of initial conditions at $t = t_{k-1}$, i.e., $\mathbf{y}_k(t_{k-1}) = \mathbf{y}_k(t_{k-1})$, is

$$\mathbf{y}_k(t) = \Phi(t, t_{k-1})\mathbf{y}_k(t_{k-1}) + \Phi(t, t_{k-1}) \int_{t_{k-1}}^t \Phi^{-1}(\tau, t_{k-1})\mathbf{B}(\tau) d\tau \quad (6)$$

where $\Phi(t, t_{k-1}) \in \mathbb{R}^{2n \times 2n}$ is the state transition matrix which is defined as

$$\Phi(t, t_0) = \mathbf{I} + \int_{t_0}^t \mathbf{A}(\tau) d\tau + \int_{t_0}^t \mathbf{A}(\tau_1) \times \left[\int_{t_0}^{\tau_1} \mathbf{A}(\tau_2) d\tau_2 \right] d\tau_1 + \dots \quad (7)$$

3 Vibration Control

The objective here is to design the required inputs that command the mechanical system, defined in Eq. (1) or (2), from a predefined state to a target state without inducing any residual vibration and satisfying other known system and input constraints. For simplicity, we consider a system that is only subjected to a single input, $f(t)$. Suppose the system input is consisted of a series of m equidistant steps such that

$$f(t) = \{c_1 \ c_2 \ \dots \ c_m\} \quad (8)$$

where c_k ($k = 1, 2, \dots, m$) is the magnitude of the constant step in the time interval $t \in [t_{k-1}, t_k]$. Upon substitution of Eq. (8) such that $\mathbf{Q}_n = \mathbf{p}f(t)$ into Eq. (6), one can write the general solution of $\mathbf{y}_k(t)$ at the time interval $t_{k-1} \leq t \leq t_k$ as

$$\mathbf{y}_k(t) = \Phi \mathbf{y}_{k0} + \Psi \mathbf{c} \quad (9)$$

where $\Psi \in \mathbb{R}^{2n \times m}$ is the matrix corresponding to the transition matrix upon performing the integration, and $\mathbf{c} \in \mathbb{R}^{m \times 1}$ is a vector containing the magnitudes of the equidistant steps. If the time of interest is $[t_0, t_f]$ where the domain is discretized into r equally spaced intervals, i.e., $t_f = t_0 + r\Delta t$, the system response at the end of the time interval, i.e., $\mathbf{y}(t_f)$, with a given known initial states, $\mathbf{y}_0 = \mathbf{y}(t_0)$, is

$$\mathbf{y}(t_f) = \mathbf{y}(t_0 + r\Delta t) = \bar{\Phi} \mathbf{y}_0 + \bar{\Psi} \mathbf{c} \quad (10)$$

where

$$\bar{\Phi} = \Phi(t_{(2r-1)/2}) \Phi(t_{(2r-3)/2}) \dots \Phi(t_{1/2}) \quad (11)$$

$$\begin{aligned} \bar{\Psi} = & \Psi(t_{(2r-1)/2}) + \Phi(t_{(2r-1)/2}) \Psi(t_{(2r-3)/2}) + \dots \\ & + \Phi(t_{(2r-1)/2}) \Phi(t_{(2r-3)/2}) \dots \Phi(t_{3/2}) \Psi(t_{1/2}) \end{aligned} \quad (12)$$

Finally, the control target can be defined as the total integral of the input that usually define its maximum capability, P , i.e.,

$$\int_{t_0}^{t_f} f(t) dt = P \quad (13)$$

Therefore, to shape an input for commanding a nonlinear system with time-varying parameter from a predefined initial state \mathbf{y}_0 to a target state \mathbf{y}_f without inducing residual vibration, the steps command should satisfy $\tilde{\Psi}\mathbf{c} = \mathbf{y}_f - \tilde{\Phi}\mathbf{y}_0$ from Eq. (10) as well as the control target from Eq. (13). Since the size of the resulting system of simultaneous linear equations is $2n + 1$ where n is the number of generalized system coordinate, then at least $m = 2n + 1$ equidistant steps are needed in Eq. (8) to satisfy the $2n$ system conditions, Eq. (10), and the one input constraint, Eq. (13).

4 Numerical Example: Overhead Crane with Simultaneous Traveling and Hoisting Motions

The proposed controlling technique is tested by controlling the induced vibrations of a payload that is traveled and hoisted/lowered by an overhead crane, Fig. 1. The following assumptions are applied: (i) the traveling and hoisting motions are restricted to a plane motion where the out-of-plane motion is neglected [8, 25], (ii) the hook and the payload is considered as a point with a mass m , (iii) the cable is massless and inextensible, (iv) the equivalent mass of the trolley (jib or slider) and the driving mechanism is M , and (v) the mechanical structure of the crane is assumed to be sufficiently rigid, i.e., neglecting the structure deformation.

The generalized coordinates of the overhead crane are the angular displacement of the payload, $\theta(t)$, the displacement of the moving trolley, $x(t)$, and the length of the hoisting cable, $l(t)$. The forces acting on the jib and the cable are $f_x(t)$ and $f_l(t)$, respectively. Using Eq. (1) with $x_1 = x - l \cos \theta$, $x_2 = l \sin \theta$, and $x_3 = 0$, the equations of motion are

$$(M + m)\ddot{x} - 2ml\dot{\theta} \cos \theta - ml\ddot{\theta} \cos \theta + ml\dot{\theta}^2 \sin \theta - m\ddot{l} \sin \theta = f_x \quad (14)$$

$$\ddot{l} - \ddot{x} \sin \theta - l\dot{\theta}^2 + g \cos \theta = -f_l \quad (15)$$

$$\ddot{\theta} + \frac{2\dot{l}}{l} + \frac{g}{l} \sin \theta = \frac{1}{l} \ddot{x} \cos \theta \quad (16)$$

Fig. 1 Schematic of overhead crane with simultaneous traveling and hoisting motions

